# Electronic structure and ferromagnetism of Mn-substituted CuAlS$_2$, CuGaS$_2$, CuInS$_2$, CuGaSe$_2$, and CuGaTe$_2$

Yu-Jun Zhao and Alex Zunger

*National Renewable Energy Laboratory, Golden, Colorado 80401, USA*

The electronic and magnetic properties of Mn doping at either cation sites in the class of I–III–VI$_2$ chalcopyrites are studied by first-principles calculation. It is found that Mn doping at the III site provides holes and stabilizes the ferromagnetic interaction between neutral Mn defects; the neutral Mn$_{Cu}^0$ also stabilizes the ferromagnetism, although it provides electrons to the conduction band, instead of holes. The ferromagnetic stability is generally weaker when the cation or the anion becomes heavier in these chalcopyrites, i.e., along the sequences CuAlS$_2$→CuGaS$_2$→CuInS$_2$ and CuGaS$_2$→CuGaSe$_2$→CuGaTe$_2$. Interestingly, CuAlO$_2$ in the chalcopyrite structure is predicted to have lower FM energy than CuAlS$_2$ despite its lighter anion and shorter bonds. In general, III site substitution gives stabler ferromagnetism than Cu substitution. Thus, the preferred growth conditions are Cu-rich and III-poor, which maximize Mn$_{III}$ replacement. In *n*-type samples, when Mn$_{III}$ is negatively charged, the antiferromagnetic coupling is preferred. In *p*-type samples, the ground state of positively charged Mn$_{Cu}^+$ is also antiferromagnetism. The main feature of the calculated electronic properties of Mn defect at either Cu or III site is explained using a simple picture of dangling bond hybride and crystal-field resonance.

## I. INTRODUCTION

Ferromagnetism in Mn-substituted semiconductors is thought to arise from the interaction of a hole with the local moment of the *d* electrons of Mn.[1,2] In II–VI's such as CdTe or ZnSe, the substitution of Mn$^{2+}$ on the *divalent* cation site introduces no holes, so ferromagnetism (FM) is not observed.[3] If the system is additionally doped by extrinsic *p*-type dopant (e.g, As-on-VI site), weak FM is observed.[4] In III–V's such as GaAs, the substitution of Mn$^{2+}$ on the *trivalent* cation site does automatically introduce a hole, so FM is observed, even without additional *p*-type doping. In the ternary pnictide system A$^{II}$M$^{IV}$X$_2^V$ such as CdGeP$_2$ or the ternary chalcopyrite system A$^I$M$^{III}$X$_2^{VI}$ such as CuAlS$_2$, the Mn can substitute either of the two cation sites.[5] In CdGeP$_2$, it was shown theoretically that isovalent substitution of Mn$^{2+}$ on the divalent Cd site produces no FM,[6] just as it is in the case of II–VI's. However, substitution on the Ge site does produce holes,[5] and along with it, predicted FM. In CuGaSe$_2$ and CuGaS$_2$, it was shown[7,8] theoretically that substitution of Mn$^{2+}$ on the Ga site does produce holes (just as in GaAs), but substitution on the monovalent Cu site is expected to produce *electrons*, and hence no FM. Since chalcopyrites easily form Cu vacancies[9] which are hole-producing acceptors, they can provide the holes necessary for FM. The foregoing discussion suggests that knowing the site preference of Mn is crucial for understanding the FM behavior. We have recently predicted the site preference of Mn in CuAlS$_2$, CuGaS$_2$, CuInS$_2$, CuGaSe$_2$, and CuGaTe$_2$, using first-principles total-energy calculations along with a set of thermodynamic chemical potential inequations.[10] We found the following:

(i) The energetic preference of Mn on the Cu site is enhanced by growth condition with high chemical potential for the column III element, whereas the preference of Mn on the M$^{III}$ site is enhanced by Cu-rich, III-poor growth conditions.

(ii) When the Fermi energy $E_F$ is near the valence band maximum (VBM), Mn$_{III}$ is charge neutral and Mn$_{Cu}$ is positively charged. Both defects are in the negative charge state when $E_F$ is close to the conduction band minimum (CBM).

(iii) The Fermi energy position affects the Mn site preference: as $E_F$ moves toward the CBM (*n*-type behavior), the solubility of Mn$^-$ on the column-III site increases. The solubility of Mn$_{Cu}^+$ decreases when $E_F$ moves from the VBM toward the CBM; it vanishes when $E_F$ passes the mid-gap. Chalcopyrites are *n*-type when they are grown anion-deficient. In this case we expect mostly Mn$_{III}$ if the sample is also Cu-rich. On the other hand, chalcopyrites are *p*-type when grown Cu-deficient. Then we expect Mn$_{Cu}$.

Having established that Mn can substitute both the Cu site and the M$^{III}$ site in chalcopyrites, we study here the electronic and magnetic consequences of both types of substitutions (for CuGaTe$_2$:Mn, Mn on Cu site is also discussed although it is not stable for all $E_F$ values). We find the following:

(i) *For Mn on the* M$^{III}$ *site* (Cu-rich, anion-poor samples), the electronic structure is $[e_+^2 t_+^3]_{CFR}(t_-^3 t_+^2)_{DBH}[e_-^0 t_-^0]_{CFR}$, where CFR and DBH stands for "crystal-field resonance" and "dangling bond hybrid," respectively. Therefore, a hole exists in a DBH state which is delocalized, and thus couples strongly to the Mn local moment. For Mn on III site the ferromagnetism stability is reduced in the sequences CuAlS$_2$→CuGaS$_2$→CuInS$_2$, and CuGaS$_2$→CuGaSe$_2$→CuGaTe$_2$. When Mn is negatively charged (by excessive donor doping), the DBH hole is filed, and antiferromagnetism (AFM) replaces FM.

(ii) *For Mn on the Cu site* (Cu-poor anion-rich samples), the electronic structure can be designated as $(t_+^3 t_-^3)_{DBH}[e_+^2 t_+^3 e_-^1]_{CFR}$, if we use the language of tetrahedral symmetry. We see that the electron exists in a localized *e*-like orbital. However, chalcopyrite has tetragonal symmetry, so the *e* levels are split into $e_a = d_{z^2}$ and $e_b = d_{x^2-y^2}$, and

TABLE I. Convergence tests for $\Delta E_{FM} = E_{FM} - E_{AFM}$ as a function of the plane wave basis energy cutoff, $E_{cut}$, and the sampling $k$ mesh, for the Al440 cases in Mn:CuAlS$_2$.

| $E_{cut}$ (eV) | $k$ mesh | $E_{FM}$ (eV) | $E_{AFM}$ (eV) | $\Delta E_{FM}$ (meV/Mn) |
|---|---|---|---|---|
| 292.16 | $2\times2\times2$ | $-312.799$ | $-312.605$ | $-97$ |
| 350.0  | $2\times2\times2$ | $-312.776$ | $-312.581$ | $-98$ |
| 400.0  | $2\times2\times2$ | $-312.795$ | $-312.599$ | $-98$ |
| 292.16 | $4\times4\times4$ | $-312.760$ | $-312.585$ | $-87$ |
| 292.16 | $6\times6\times6$ | $-312.758$ | $-312.577$ | $-90$ |

the $t_2$ levels split into $t_a = d_{xz}; d_{yz}$ and $t_b = d_{xy}$. We find that the electron actually resides in a level that mixes $e_b$ with $t_b$ character, rendering to it some delocalized $t_2$-like character. Thus, Mn on Cu site also introduces ferromagnetism. The ferromagnetic stability for Mn on the Cu site is generally lower than for Mn on the III site, with minor exceptions. The order of ferromagnetic stability for Mn-on-Cu (for Mn atoms being fourth neighbors) is reduced in the series CuGaSe$_2 \rightarrow$ CuGaS$_2 \rightarrow$ CuGaTe$_2 \rightarrow$ CuAlS$_2 \rightarrow$ CuInS$_2$.

(iii) Ferromagnetism depends on the orientation of the Mn atoms within the chalcopyrite lattice. The highest stabilization exists for Mn atoms oriented along the $\langle 110 \rangle$ direction, e.g., one Mn at $(0,0,0)$ and one at $(\frac{1}{2},0,\frac{1}{2})a$ (the first neighbor) or at $(0,0,0)+(1,1,0)a$ (fourth neighbor). The highest FM stabilization (239 meV/Mn) exists for the first neighbor Mn–Mn on the Cu site of CuAlS$_2$.

## II. METHOD OF CALCULATION

We use the pseudopotential momentum-space total-energy method[11] within the generalized gradient approximation of PW91 formulas,[12] and the ultrasoft pseudopotentials of Vanderbilt,[13] as implemented by the VASP code.[14] The electronic properties of Mn doping at the M$^{III}$ site or the Cu site are studied using a single Mn atom in a 64-atom supercell. The magnetic coupling between Mn atoms are simulated by a *pair* of Mn atoms in a 64-atom supercell. There are several possible configurations for a Mn pair in the supercell, distinguished by the vector (in unit of $a/4$) connecting one Mn at $(0,0,0)$ with another one at $(2,0,2)$, or $(4,0,0)$, or $(2,2,4\eta)$, *etc*, where $\eta = c/2a$. These are, respectively, the first, second, third nearest neighbors, and are labeled as Al202, Al400, and Al224, respectively. Analogous notation is used for Mn substituting Cu.

We use a plane wave basis set with and energy cutoff of 292.16 eV and a $k$ mesh of $4\times4\times4$ following Monkhorst–Pack scheme.[15] Convergence tests (Table I) were carried out for CuAlS$_2$:Mn in the Al440 case, showing that there are no remarkable changes in the magnetic stability energy, $\Delta E_{FM} = E_{FM} - E_{AFM}$, when the energy cutoff for the basis is raised to 400 eV. Also, $\Delta E_{FM}$ changes only 3 meV when the sampling $k$ mesh is increased to $6\times6\times6$.

We will discuss the "transition energy" $E(q/q')$, which is the change in total energy when the system changes its charge state via altering the occupation of the gap levels. Such acceptor $E(0/-)$ or donor $E(0/+)$ energies are calculated as[9]

$$E_\alpha(q/q') = [E(\alpha,q) - E(\alpha,q')]/(q'-q). \quad (1)$$

Here, $E(\alpha,q)$ and $E(\alpha,q')$ are the total energy of the defect system at different charge states. $E_\alpha(q/q')$ is relative to the valence band maximum (VBM), which is calculated by the total energy difference $E(0) - E(+)$ of the *defect-free* system. Makov–Payne correction[16] up to the quadrupole term is applied to the charged systems. No local density approximation (LDA) gap band correction is done in this calculation.

We choose to display the transition energies on an absolute energy scale. This requires the calculation of band offsets of different chalcopyrite. The valence band offsets are calculated as[17]:

$$\Delta E = [E_v - \langle V \rangle]_B - [E_v - \langle V \rangle]_A + [\langle V \rangle_B - \langle V \rangle_A]_{A/B}. \quad (2)$$

The first term on the right-hand side is the energy of the valence-band edge in pure bulk B with respect to the averaged potential $\langle V \rangle_B$ at the core area of the Cu atom. The second term is the analogous quantity for material A. The third term in Eq. (2) is the difference in the average potential at Cu core area on either side (but far from) the A/B interface. The interface supercells of A and B are simulated by eight layers A and B, i.e., (CuAlS$_2$)$_4$/(CuGaS$_2$)$_4$. The lattice constant of $a$ is given by Vegard's rule:[18] $a(x) = (1-x)a_A + xa_B$, and $c$ is determined by fixing the crystal volume. The error for $\Delta E$ is within 0.04 eV when supercell is increased to A$_6$B$_6$, as tested for CuAlS$_2$ and CuGaS$_2$.

## III. THE ELECTRONIC STRUCTURE OF SINGLE Mn SUBSTITUTIONS IN CHALCOPYRITES

In *tetrahedral* systems such as CdTe or GaAs, substitutional Mn leads to $a_1 + t_2 + e$ representations.[19] However, chalcopyrite is *tetragonal*, not tetrahedral. Indeed, the anion S in CuAlS$_2$ is coordinated by two Cu atoms and two Al atoms. Consequently, the $t_2$ state splits into doubly degenerated $t_a = d_{xz}; d_{yz}$ and singly degenerated $t_b = d_{xy}$, whereas the $e$ state splits into $e_a = d_{z^2}$, and $e_b = d_{x^2-y^2}$. We will still use the tetrahedral nomenclature for discussing similarity with Mn in binary semiconductors, and revert to the tetragonal notation where needed. In the following discussion on electronic structure, we use CuAlS$_2$:Mn as an example.

### A. Single Mn substituting the column III site

The calculated equilibrium Mn–X$^{VI}$ bond lengths for Mn substituting the column III site are listed in Table II, where they are compared with the ideal M$^{III}$-X$^{VI}$ bond length, in the

TABLE II. The total energy difference between antiferromagnetic and ferromagnetic states, $\Delta E_{FM} = E_{FM} - E_{AFM}$. for two Mn atoms in a 64 atom supercell of $CuAlS_2$, $CuGaS_2$, $CuInS_2$, $CuGaSe_2$, and $CuGaTe_2$. "Mn sites" are (0,0,0) plus a Mn at the denoted site. The total energy of the most stable phase is set to zero for $Mn_{III}$ or $Mn_{Cu}$ at the same charge state. The bond length of Mn–VI for FM phase is also listed, with the variations in parentheses for nonequivalent bonds. We also give the bond length for the pure chalcopyrite ("ideal").

| Host | Mn sites (charge) | Bond length (Å) | | $E_{FM}$ (meV) | $E_{AFM}$ (meV) | $\Delta E_{ex}$ (meV/Mn) | Total moment ($\mu_B$) |
|---|---|---|---|---|---|---|---|
| | | Mn-VI | Ideal | | | | |
| $CuAlS_2$ | Al202 | 2.32(2) | | 6 | 201 | −97 | 4.0 |
| | Al400 | 2.35 | 2.27 | 91 | 168 | −38 | 4.0 |
| | Al224 | 2.34(1) | | 33 | 173 | −70 | 4.0 |
| | Al440 | 2.33 | | 0 | 174 | −87 | 4.0 |
| | Cu022 | 2.56(21) | | 0 | 478 | −239 | 4.0 |
| | Cu400 | 2.37(1) | 2.32 | 493 | 534 | −21 | 4.0 |
| | Cu224 | 2.38(1) | | 483 | 535 | −26 | 4.0 |
| | Cu440 | 2.36 | | 460 | 547 | −43 | 4.0 |
| | Al440($q=2-$) | 2.36 | | 25 | 0 | 12 | 5.0 |
| | Cu022($q=2+$) | 2.41(3) | | 72 | 0 | 36 | 5.0 |
| | CuAl444 | 2.36 | | 0 | 0 | 0 | 5.0 |
| $CuGaS_2$ | Ga202 | 2.32(2) | 2.30 | 21 | 183 | −81 | 4.0 |
| | Ga440 | 2.33 | | 0 | 161 | −81 | 4.0 |
| | Cu022 | 2.36(6) | 2.30 | 0 | 91 | −46 | 4.1 |
| | Cu440 | 2.33 | | 32 | 170 | −69 | 4.0 |
| $CuInS_2$ | In202 | 2.38(2) | 2.50 | 48 | 182 | −67 | 4.0 |
| | In440 | 2.39 | | 0 | 135 | −68 | 4.0 |
| | Cu022 | 2.38(2) | 2.30 | 122 | 93 | 15 | 4.5 |
| | Cu440 | 2.35 | | 0 | 74 | −37 | 4.5 |
| $CuGaSe_2$ | Ga202 | 2.44(2) | 2.43 | 21 | 160 | −70 | 4.1 |
| | Ga440 | 2.44 | | 0 | 123 | −61 | 4.0 |
| | Cu022 | 2.46(3) | 2.39 | 29 | 104 | −38 | 4.1 |
| | Cu440 | 2.44 | | 0 | 160 | −80 | 4.1 |
| $CuGaTe_2$ | Ga202 | 2.63(1) | 2.63 | 50 | 150 | −50 | 4.0 |
| | Ga440 | 2.63 | | 0 | 115 | −58 | 4.0 |
| | Cu022 | 2.62(1) | 2.55 | 28 | 85 | −29 | 4.0 |
| | Cu440 | 2.61 | | 0 | 127 | −64 | 4.0 |

pure host chalcopyrites. We calculated the ideal bond length, Al–S (2.27 Å), Ga–S (2.30 Å), Ga–Se (2.43 Å), Ga–Te (2.63 Å), and In–S (2.50 Å), in very good agreement (less than 2% difference) with the measured bond length listed in Ref. 20. Substitution of Mn on the column III site creates a *shorter* bond with S in $CuAlS_2$, a *longer* bond in $CuInS_2$, but in $CuGaS_2$, $CuGaSe_2$, or $CuGaTe_2$, the bonds are unchanged by Mn substitution, suggesting a similar tetrahedral radius for Ga and Mn in those compounds.

Figure 1(a) shows the Mn $3d$ projected local density of states (LDOS). Going from deeper to shallower levels, we see the sequence $e_+^{CFR} \rightarrow t_+^{CFR} \rightarrow t_+^{DBH} \rightarrow t_-^{DBH} \rightarrow e_-^{CFR} \rightarrow e_+^{CFR}$. The labeling "dangling bond hybride" (DBH) and "crystal-field resonance" (CFR) will be explained in the following and Figs. 2(a) and 2(b) show, respectively, the spin-up and spin-down wave function square at $\Gamma$ of these states. We see the following:

(i) The $e^{CFR}$ states are $e$-like, i.e., have lobes that point in-between the nearest neighbors. Those state are highly localized on Mn, and can be thought of as nonbonding. The lowest state $e_+^{CFR}$ lies deep inside the host valence band and is occupied by two spin-up electrons. The higher state $e_-^{CFR}$ lies deep inside the conduction band and is empty.

(ii) The $t^{CFR}$ states are $t_2$-like, i.e., have lobes that point to the nearest neighbors, and can be thought of as highly localized bonding states. The lowest state $t_+^{CFR}$ lies deep in the valence band and is occupied by three spin-up electrons. The higher state, $t_-^{CFR}$, lies in the conduction band, and is empty. The $e_+^{CFR}$ is lower in energy by about 0.29 eV than $t_+^{CFR}$ due to the tetrahedral crystal field splitting. These states are further crystal-field split in the tetragonal symmetry by 0.01 eV for spin up, and by 0.07 eV for spin down at $\Gamma$ point.

(iii) The state designated $t^{DBH}$ lies near the Fermi energy. It is a Mn, $d$-S,$p$ hybride, and thus shows more extended wave functions than the $t^{CFR}$, which is nearly pure $d$. In the neutral charge state, the spin-*down* $t_-^{DBH}$ is occupied by three electrons, whereas the spin-*up* $t_+^{DBH}$ is occupied by two electrons, and thus carries the hole.
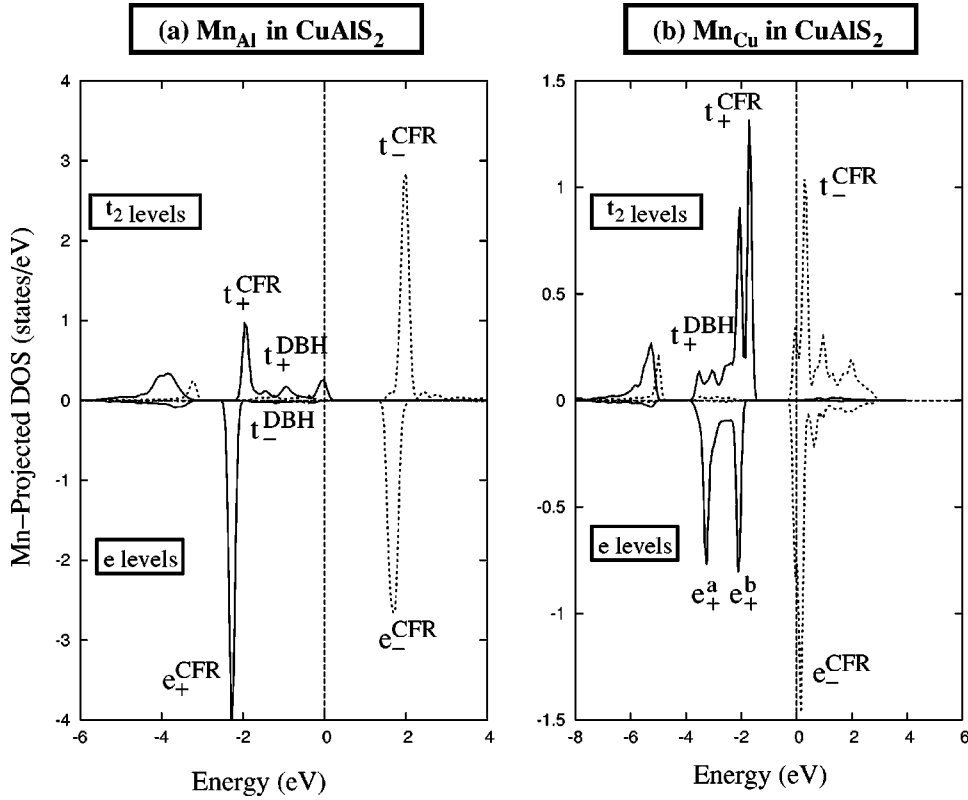
FIG. 1. Projected $e$ and $t$ DOS levels for $Mn_{Al}^0$ and $Mn_{Cu}^0$ in a 64 atom supercell of $CuAlS_2$ in a sphere radius of 1.17 Å. Spin up DOS are shown in solid lines, whereas spin down in dashed line. The Fermi level is at $E = 0$.

The overall electron configurations of $Mn_{Al}^0$ can thus be designated as $[e_+^2 t_+^3]_{CFR}(t_-^3 t_+^2)_{DBH}[e_-^0 t_-^0]_{CFR}$. The total moment is thus $\mu = 2 + 3 - 3 + 2 = 4$. Since the CFR states are Mn-localized and carry five spin-up electrons, whereas the DBH is more extended, and carries a hole, such a ground state is often designated as "$d^5$+ hole." It is interesting to compare the degree of localization of up-spin vs down spin states. Figure 2 shows that $t_-^{DBH}$ is more delocalized than $t_+^{DBH}$.

Since $Mn_{Al}^0$ contains a hole at the $t_+^{DBH}$ state, raising the Fermi energy $E_F$ via $n$-type doping will lead to the capture of an electron from the Fermi sea into this orbital, transforming $Mn_{Al}^0$ to $Mn_{Al}^-$. The change in *total* energy for this acceptor reaction is the acceptor transition energy $E(0/-)$, and is calculated as explained in Sec. II and Eq. (2). Figure 3(a) shows the calculated acceptor level for $Mn_{III}$ in a few chalcopyrites. We see that all the acceptor levels of $Mn_{III}$ are ranging between 180 and 350 meV. The acceptor level becomes progressively shallower along the series $CuGaS_2 \rightarrow CuAlS_2 \rightarrow CuGaSe_2 \rightarrow CuGaTe_2 \rightarrow CuInS_2$.

The electronic structure of $Mn_{Al}$ obtained through numerical calculations [Figs. 1(a) and 2 can be explained qualitatively by a simple model introduced in the context of binary solids in Ref. 19—Fig. 4(a)]. We describe the electronic structure of $Mn_{Al}$ as a result of coupling between the $(e_+, t_+)$ and $(e_-, t_-)$ $d$-orbitals of the Mn ion embedded in a crystal field, with the orbitals formed by an Al vacancy in $CuAlS_2$. These vacancy orbitals are actually dangling bonds of S surrounding the vacant Al site. Calculation of $V_{Al}$ in $CuAlS_2$ shows that at $\Gamma$, the dangling bond orbitals are at $E_{VBM} + 0.05$ eV, i.e., slightly above the VBM. If the energy

of the cation vacancy dangling bonds lies between the energies of up-spin and the down-spin Mn $3d$ orbitals [Fig. 4(a)], one obtains a level scheme as shown at the center of Fig. 4(a). The spin-up impurity orbital $t_+(d)$ hybridize with the spin-up host dangling bond $t_+(p)$, to form the bonding $t_+^{CFR}(dp)$ and the anti-bonding $t_+^{DBH}(dp)$ levels. The bonding orbital contains more $t_+(d)$ character, whereas the antibonding orbital contains more $t_+(p)$ character. Analogously, the spin-down impurity orbital $t_-(d)$ hybridizes with the spin-down host dangling bond $t_-(p)$ to form the bonding $t_-^{CFR}(dp)$ and the antibonding $t_-^{DBH}(dp)$. Note that $t_-^{DBH}$ is below $t_+^{DBH}$ ("negative DBH exchange splitting") since $t_-^{DBH}$ is repelled downward [by $t_-(d)$] more than $t_+^{DBH}$ is repelled upward [by $t_+(d)$]. In contrast, $t_+^{CFR}$ is below $t_-^{CFR}$ ("positive CFR exchange splitting"). Thus, the direction of spin polarization on the Mn site (decided by CFR) is opposite to the direction of spin polarization on the nearest anion sites (decided by DBH). This is the fingerprint of antiferromagnetic coupling between Mn $3d$ and the anion $p$ orbitals. Since the host dangling bonds do not have an $e$-like representation in the relevant energy range, the ionic $e_-(d)$ and $e_+(d)$ levels are unperturbed, and appear as $e_-^{CFR}$ and $e_+^{CFR}$. Thus, the simple model of Fig. 4(a) reproduces the essential feature of the full first-principles calculations.

### B. Single Mn substituting the Cu site

The Mn–$X^{VI}$ bond lengths for Mn substituting Cu site are listed in Table II, where they are compared with the ideal Cu–$X^{VI}$ bond lengths in the pure host chalcopyrites. We find the ideal bond length, Cu–S (2.32±0.02 Å), Cu–Se (2.39

**(a)** Spin–up Wavefunction Square for $Mn_{Al}^0$ in $CuAlS_2$
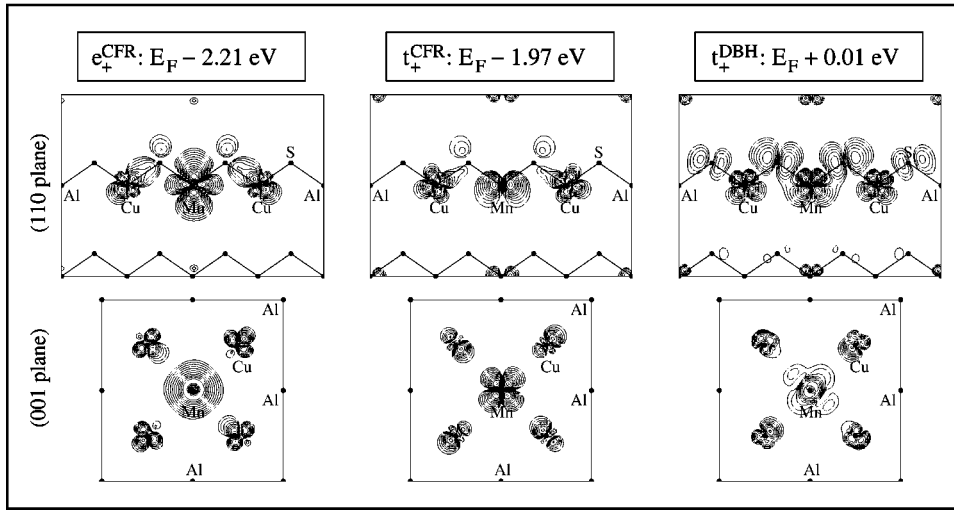


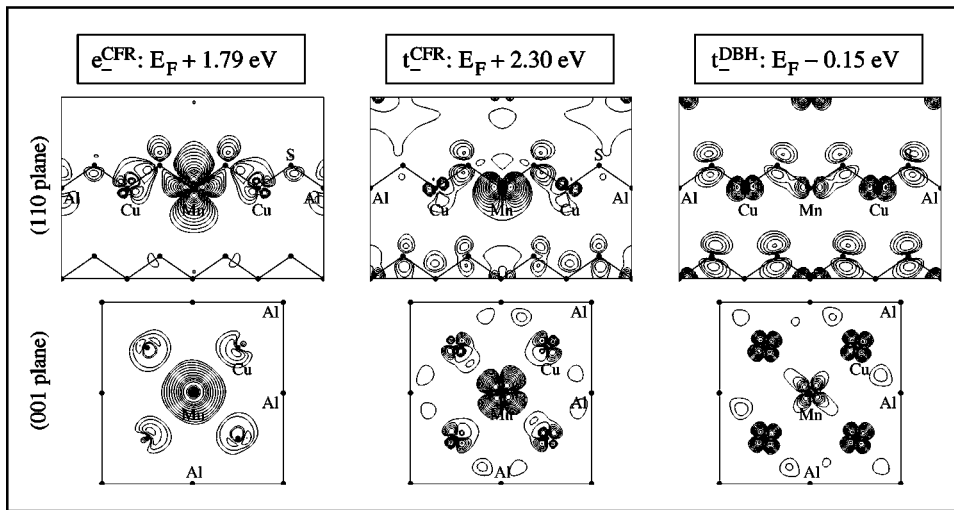**(b)** Spin–down Wavefunction Square for $Mn_{Al}^0$ in $CuAlS_2$



FIG. 2. $\Gamma$-point wave function square for spin-up (a) and spin-down (b) in the (110) and (001) planes for $e^{CFR}$ (only $d_{z^2}$ is shown), $t^{CFR}$ (only $d_{xy}$ is shown), and $t^{DBH}$ states of $Mn_{Al}^0$ in $CuAlS_2$. The density contours start from $10^{-3} e/$ Å$^3$ and increase successively by a factor of $\sqrt{3}$.

Å), and Cu–Te (2.55 Å), in good agreement with the experimental ones.[20] Mn substitution on the Cu site creates uniformly longer bonds than the host Cu–X bond, indicating that the Mn tetrahedral radius is larger than that of Cu.

Figure 1(b) shows the Mn $3d$ projected LDOS of neutral $Mn_{Cu}$, and Fig. 5 shows the wave function square at $\Gamma$ point. Here the crystal-field splitting due to the tetragonal field is larger than in $Mn_{Al}$, being 0.09 eV for $e_+$ orbitals and 0.25 eV for $t_+$ orbitals at $\Gamma$ point. These states are further separated at off-$\Gamma$ point. We see the following:

(i) The $e_+^{CFR}$ states are split clearly into $e_+^a = d_{z^2}$ and $e_+^b = d_{x^2-y^2}$, both being highly localized valence band states occupied by a total of two spin-up electrons. The $e_-^{CFR}$ are localized orbitals deep inside the conduction band, and are empty.

(ii) The $t_+^{CFR}$ levels are split into two components by the crystal field, and are occupied by three spin-up electrons. The spin-down $t_-^{CFR}$ counterpart are unoccupied states in the conduction band.
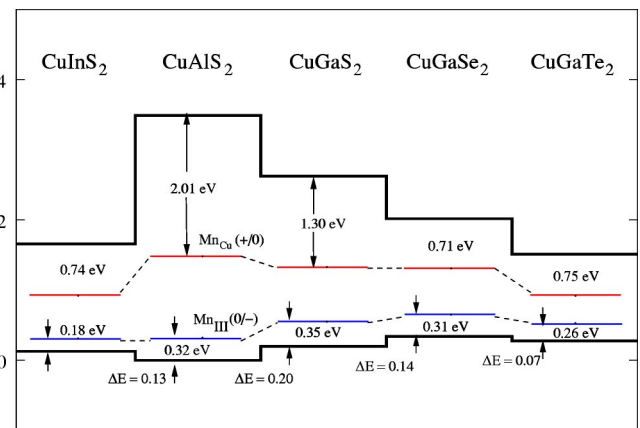


FIG. 3. Acceptor $(0/-)$ and donor $(0/+)$ transition energy, plotted with respect to the band edge that are aligned according to the calculated band offsets. The values of band gap are from experiments (Ref. 29).
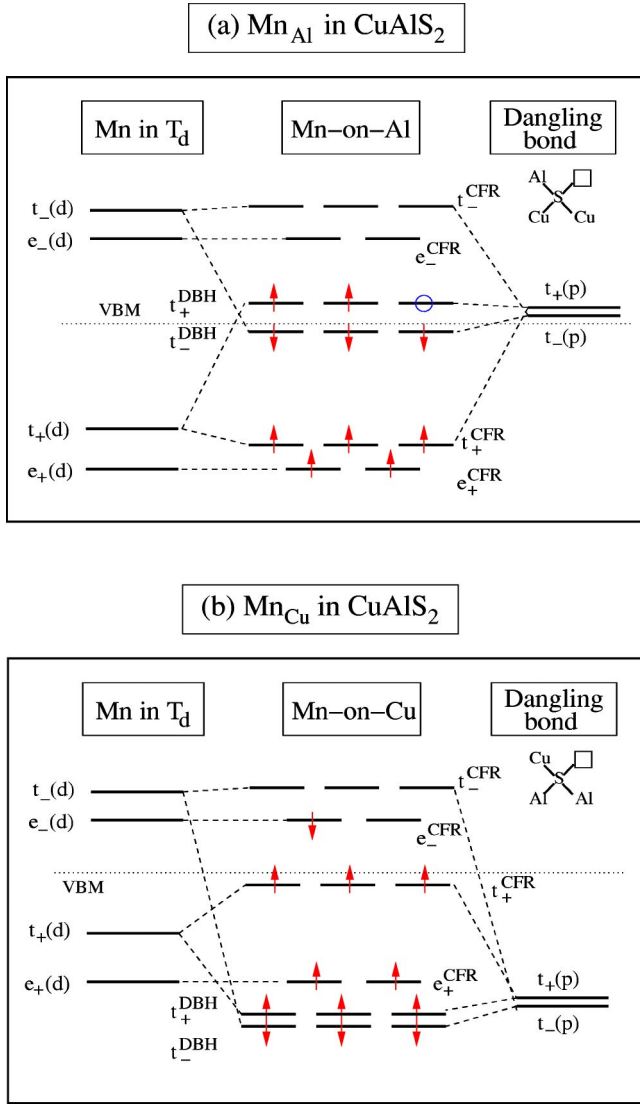
FIG. 4. The energy level diagram of $Mn_{Al}$ and $Mn_{Cu}$ in $CuAlS_2$. The level splitting due to tetragonal structure is not shown in this diagram.

(iii) In the case of $Mn_{Cu}$ we have the DBH electrons deep in the valence band below $t_+^{CFR}$, whereas in $Mn_{Al}$ they were near the VBM, above $t_+^{CFR}$. The $t^{DBH}$ states, shown around $E_{VBM} - 1.8$ eV, are occupied by three spin-up and three spin-down electrons. Inspection of the LDOS in the S next to Mn show that those DBH states have small spin splitting, are mostly anion-like, and are mostly contributed from off-$\Gamma$ point wave functions (and thus are not seen in the $\Gamma$ point wave function plot of Fig. 5). The order of levels for $Mn_{Cu}^0$, going from deep to shallower levels is thus, $t_+^{DBH} \to t_-^{DBH} \to e_+^{CFR} \to t_+^{CFR} \to e_-^{CFR}$, quite different from the order in $Mn_{Al}^0$. The formal configuration is thus $(t_+^3 t_-^3)_{DBH} [e_+^2 t_+^3 e_-^1]_{CFR}$ with a moment of $3 - 3 + 2 + 3 - 1 = 4 \ \mu_B$ and an electron in $e_-$. However, because the tetragonal crystal-field splitting of the $e$ and $t_2$ levels is large in $Mn_{Cu}$, there is a secondary coupling between the split components $e_b(d_{x^2-y^2})$ and $t_b(d_{xy})$, which is allowed by the reduced symmetry due to the Mn defect. Thus,

the electron resides in a level that is $(\frac{2}{3} d_{x^2-y^2})$ and $(\frac{1}{3} d_{xy})$. Consequently, the electron at $E_F$ does have some $t_2$-like character. Figure 3 shows that the donor level of $Mn_{Cu}$ is very deep (more than 710 meV) for all these chalcopyrites.

The electronic structure of $Mn_{Cu}$ obtained through numerical calculations can be explained qualitatively by a simple model [Fig. 4(b)]. Here, we first note that whereas the dangling bond $t_2$ orbital of the Al vacancy in $CuAlS_2$ lies *above* the VBM, that due to a Cu vacancy lies about 1.90 eV *below* the host VBM.[21] Thus, in Fig 4(b), we placed the $t(p)$ level below the $t(d)$ level of Mn. This order of unperturbed levels produces the level scheme seen in our calculation. The $t_+(p)$ level of the host hybridize with the $t_+(d)$ level of the impurity to give the deep $t_+^{DBH}$ bonding level, and the $t_+^{CFR}$ antibonding level. Note that for $Mn_{Al}$ the order is reverted, since $t_+(d)$ is below $t_+(p)$. Similarly, the $t_-(p)$ level of the host hybridize with the $t_-(d)$ level of the impurity to yield the bonding $t_-^{DBH}$ and antibonding $t_-^{CFR}$. Like in $Mn_{Al}$, here too the $e_-^{CFR}$ and $e_+^{CFR}$ levels are mostly unperturbed. Thus, the fact that the *host* dangling bond $V_{Cu}$ is deeper than the host dangling bond $V_{Al}$ leads to the different level ordering for Mn-on-Al [Fig. 4(a)] and Mn-on-Cu [Fig. 4(b)].

## IV. FERROMAGNETIC AND ANTIFERROMAGNETIC ENERGIES FOR TWO Mn IN CHALCOPYRITES

So far we have considered a single Mn atom per supercell, for studying the electronic structure. To study the magnetic ground state, we have placed *two* Mn atoms in a 64 atom chalcopyrite supercell, and computed the total energies for the ferromagnetic $E_{FM}$ and antiferromagnetic $E_{AFM}$ spin arrangement. We studied several possible configurations for a Mn pair in these chalcopyrites. The calculated $\Delta E_{FM} = E_{FM} - E_{AFM}$ of different Mn pair configurations for $CuAlS_2$, $CuGaS_2$, $CuInS_2$, $CuGaSe_2$, and $CuGaTe_2$ are listed in Table II. The total energy of the most stable configuration for Mn doped at III site or at the Cu site is taken in Table II as reference energy. The pseudopotential results using ultrasoft potentials are in excellent agreement with the previous all-electron full-potential linearized augmented plane wave (FLAPW) calculations.[22,8] The latter calculation gives $\Delta E_{FM}$ of $-77$ and $-64$ meV for Ga440 in $CuGaS_2$ and $CuGaSe_2$, respectively, whereas current pseudopotential calculation gives $-81$ and $-61$ meV, respectively. This indicates that the pseudopotential calculation is appropriate to give a reasonable description of the magnetic properties of Mn doped chalcopyrites. Table II shows the following:

(i) *Chemical trends of FM:* The ferromagnetic state is favored ($\Delta E_{FM} < 0$) for all the *neutral* charge states when Mn substitutes either the Cu or the column III site.[23] In general, III-substitution gives stabler FM than Cu-substitution. Thus, the preferred growth conditions for FM are Cu-rich and III-poor. The sample should not be strongly *n*-type (i.e., avoid excessive S deficiency) because then the acceptor will be filled, leading to AFM.
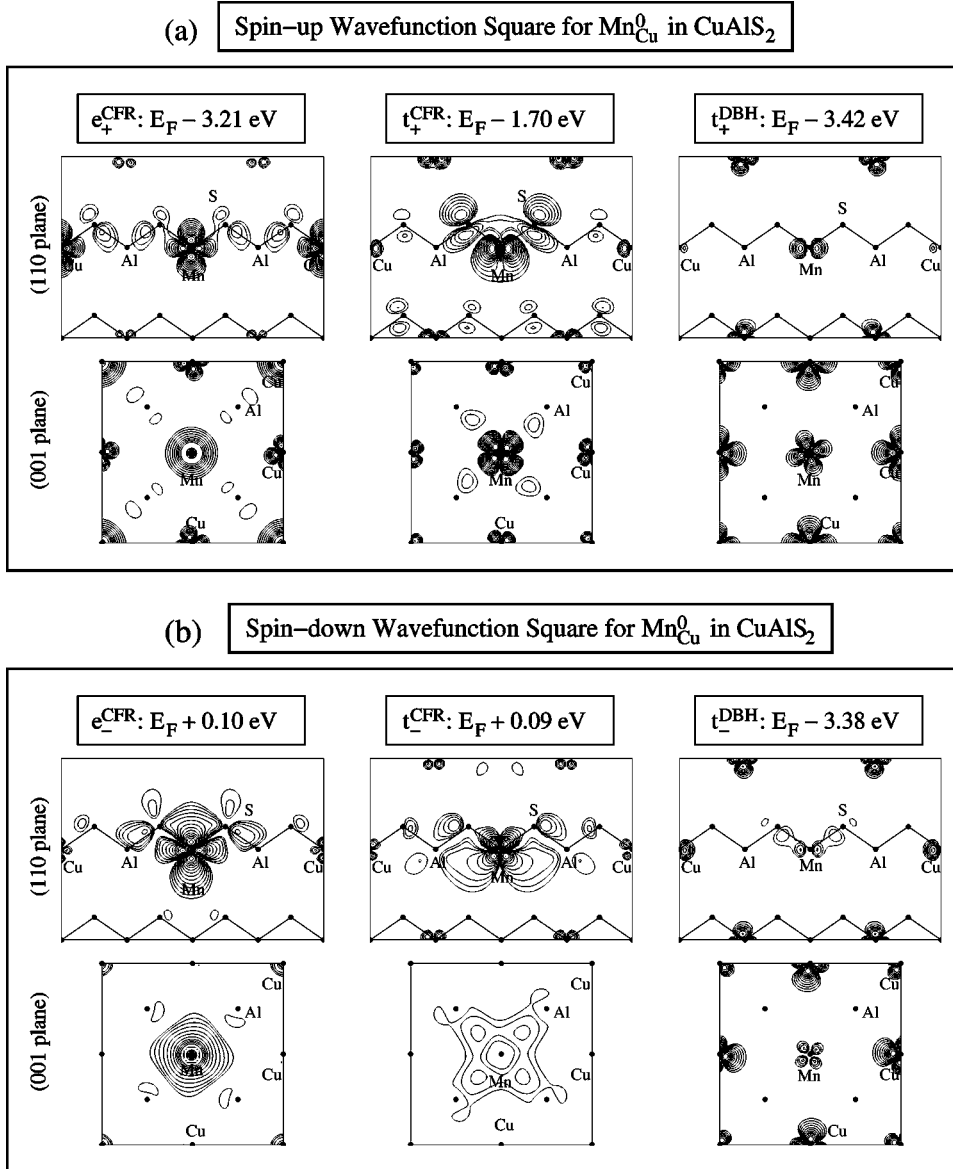
FIG. 5. $\Gamma$-point wave function square for spin-up (a) and spin-down (b) in the (110) and (001) planes for $e^{CFR}$ (only $d_{z^2}$ is shown), $t^{CFR}$ (only $d_{xy}$ for spin-up and degenerated $d_{yz}$ and $d_{xz}$ for spin-down are shown), and $t^{DBH}$ states of $Mn^0_{Cu}$ in $CuAlS_2$. The density contours start from $10^{-3}e/$ Å$^3$ and increase successively by a factor of $\sqrt{3}$.

(ii) *For column III site substitution*, considering the Mn pair at first neighbor, the FM decreases in the sequence $CuAlS_2 \rightarrow CuGaS_2 \rightarrow CuGaSe_2 \rightarrow CuInS_2 \rightarrow CuGaTe_2$. In other words, the ferromagnetic stability is weaker when the cation or the anion becomes heavier. Moreover, the bond length of $Mn_{M^{III}}$ also becomes larger along the above series. By comparing the $Mn_{III}$ acceptor levels, we find that the FM is more stable for a $Mn_{III}$ pair when the acceptor level is deeper (cf. Fig 3). One might conclude from the above scaling that moving to a lighter anion (e.g., Se→S→O) with shorter bonds would enhance FM. However, calculations on the chalcopyrite structure of $CuAlO_2$ (with the calculated lattice constants, $a=4.640$ Å, $c=8.364$ Å) show $\Delta E_{ex}=-52.9$ and $+25.7$ meV/Mn for Al440 and Al202 configuration, respectively, both higher than the corresponding values $-87$ and $-97$ meV/Mn for $CuAlS_2$ (cf Table II). Thus, the inverse scaling of $\Delta E_{ex}$ vs bond length[1] does not apply, since $R_{Mn-O}=1.92-2.05$ Å, whereas $R_{Mn-S}=2.33$ Å, yet $CuAlS_2$ has stabler FM.

(iii) *For Cu site substitution*, the chemical trend of ferromagnetic stability is not regular. For the nearest neighbor Mn pair, the stability decreases along $CuAlS_2 \rightarrow CuGaS_2 \rightarrow CuGaSe_2 \rightarrow CuGaTe_2$ and $CuInS_2$; whereas for the fourth nearest neighbor, it decreases along the $CuGaSe_2 \rightarrow CuGaS_2 \rightarrow CuGaTe_2 \rightarrow CuAlS_2$ and $CuInS_2$ series.

(iv) *Crystallographic anisotropy of FM:* The ferromagnetic stability may depend on the orientation of the Mn atoms in the lattice. For example, the ferromagnetic stability of second (400) and third (224) neighbor $Mn_{Al}$ pairs is weaker than that of fourth neighbor (440) in $CuAlS_2$, which is along the $\langle 110 \rangle$ direction as the nearest neighbor. This is also true for $Mn_{Cu}$ pairs in $CuAlS_2$. The stronger ferromagnetic stability when the Mn–Mn pair is oriented along $\langle 110 \rangle$ also occurs in GaAs when Mn doping on Ga site.[24] It is interesting that the ferromagnetic stability of $Mn_{Cu}-Mn_{Cu}$ nearest neighbor pair is weaker than that of fourth nearest neighbor (440) except in $CuAlS_2$. The strong ferromagnetic coupling of Cu022 in $CuAlS_2$ is due to the shortening of the Mn-Mn

distance: the Mn–Mn distance for Cu022 is reduced to 2.83 Å from their ideal distance (3.77 Å), and one bonded S atom is pushed away from each Mn by more than 0.40 Å. In contrast, for the AFM phase of Cu022 in CuAlS$_2$, the Mn–Mn distance is 3.57 Å, not far from its ideal value.

(v) *Charge dependence of FM:* When the charge state of Mn$_{Al}^q$ changes from $q=0$ (holes in the DBH) to $q=-1$ (no holes), the FM disappears, and the ground state is AFM. The same is true for Mn$_{Cu}^q$ when a changes from $q=0$ (electron carriers in conduction band) to $q=+1$ (no electron carriers). This means that when the material is doped excessively *n*-type, the hole will disappear and FM will vanish. In chalcopyrites, *n*-doping is caused by anion vacancies,[9] or H,[25,26] or Cd/Zn impurities. Interestingly, a recent experiment[27] found that Mn ions are coupled antiferromagnetically in CuIn$_{1-x}$Mn$_x$S$_{2-\delta}$, grown under strong S-deficient condition. Understanding of the magnetism in this sample will require an independent measurement of hole and electron carrier concentration.

(vi) *Mn clustering:* The tendency for Mn to cluster can be measured by the clustering energy $\delta E(n)$,[28] which is defined as the energy difference between *n* substitutional Mn atoms surrounding an anion site ($0 \le n \le 4$) and *n* isolated, well-separated constituents. Thus, $\delta E(n) = [E(n) - E(0)] - n[E(1) - E(0)]$, where $E(n)$ is the total energy of the supercell with anion-centered clusters of *n* Mn atoms for Mn substituting the III site. For $n=2$, we calculate $\delta E(n) = -0.12, -0.05, 0.02, 0.01, 0.04$ eV per Mn pair, whereas

for Mn on Cu site we find $\delta E(n) = -0.53, -0.07, 0.05, 0.18, 0.06$ eV for CuAlS$_2$, CuGaS$_2$, CuInS$_2$, CuGaSe$_2$, and CuGaTe$_2$, respectively. Therefore, Mn clustering is likely to occur in CuAlS$_2$, while it is not clear in other chalcopyrites.

## V. SUMMARY

In summary, we find that the electronic sturcture for Mn at the III site in I–III–VI$_2$ chalcopyrites can be designated as $[e_+^2 t_+^3]_{CFR}(t_-^3 t_+^2)_{DBH}[e_-^0 t_-^0]_{CFR}$. Therefore, Mn doping at III site provides holes and stabilizes the ferromagnetic coupling between Mn ions. The ferromagnetism is reduced when the cation III or the anion VI becomes heavier. When Mn substitutes Cu site, its electronic structure can be designated as $(t_+^3 t_-^3)_{DBH}[e_+^2 t_+^3 e_-^1]_{CFR}$. The electron in the conduction band is ineed a mixture of *e* and some delocalized *t* character, and thus introduces FM. In general, the ferromagnetic stability for Mn on III site is higher than for Mn on the Cu site. Therefore, Cu-rich and III-poor growth conditions are preferred for stronger FM. When the charge state of Mn$_{III}^q$ changes from $q=0$ to $q=-1$, the FM disappears, and the ground state is AFM; the same is true for Mn$_{Cu}^q$ when a changes from $q=0$ to $q=+1$.

## ACKNOWLEDGMENT

[1] T. Dietl, H. Ohno, J. Cibert, and D. Ferrand, Science **287**, 1019 (2000).

[2] T. Dietl, H. Ohno, and F. Matsukura, Phys. Rev. B **63**, 195205 (2001).

[3] *Diluted Magnetic Semiconductors, Semiconductors and Semimetals*, edited by J. K. Furdyna and J. Kossut (Academic, Boston, 1986), Vol. 25.

[4] T. Dietl *et al.*, Phys. Rev. B **63**, 085201 (2001).

[5] P. Mahadevan and A. Zunger, Phys. Rev. Lett. **88**, 047205 (2002).

[6] Y.-J. Zhao, W.T. Geng, A.J. Freeman, and T. Oguchi, Phys. Rev. B **63**, 201202 (2001).

[7] Y.-J. Zhao and A.J. Freeman, J. Magn. Magn. Mater. **246**, 145 (2002).

[8] S. Picozzi, Y.-J. Zhao, A. J. Freeman, and B. Delley, Phys. Rev. B **66**, 205206 (2002).

[9] S.B. Zhang, S.-H. Wei, A. Zunger, and H. Katayama-Yoshida, Phys. Rev. B **57**, 9642 (1998).

[10] Y.-J. Zhao and A. Zunger, Phys. Rev. B **69**, 075208 (2004).

[11] J. Ihm, A. Zunger, and M.L. Cohen, J. Phys. C **12**, 4409 (1979).

[12] J.P. Perdew and Y. Wang, Phys. Rev. B **45**, 13 244 (1992).

[13] D. Vanderbilt, Phys. Rev. B **41**, 7892 (1990).

[14] G. Kresse and J. Hafner, Phys. Rev. B **47**, RC558 (1993); G. Kresse and J. Furthmüller, *ibid.* **54**, 11 169 (1996).

[15] H.J. Monkhorst and J.D. Pack, Phys. Rev. B **13**, 5188 (1976).

[16] G. Makov and M.C. Payne, Phys. Rev. B **51**, 4014 (1995).

[17] R.G. Dandrea, C.B. Duke, and A. Zunger, J. Vac. Sci. Technol. B

**10**, 1744 (1992).

[18] L. Vegard, Z. Phys. **5**, 17 (1921).

[19] A. Zunger, Solid State Phys. **39**, 275 (1986).

[20] J.E. Jaffe and A. Zunger, Phys. Rev. B **29**, 1882 (1984).

[21] When the $V_{Cu}^0$ $t_2$ *orbital* (occupied by five electrons) is calculated to be below the VBM, an electron from the VBM drops into this level. The acceptor *transition* energy is then just above the VBM. Experimentally, it is at $E_v + 0.19$ eV [see I. Aksenov, N. Nishikawa, and K. Sato, J. Appl. Phys. **74**, 3811 (1993)].

[22] A.J. Freeman and Y.-J. Zhao, J. Phys. Chem. Solids **64**, 1453 (2003).

[23] The exception to FM is Cu022 case in CuInS$_2$; however here the LDA gap vanishes and the local moment is 4.5 $\mu_B$, not the expected 4.0 $\mu_B$, so the result may be clouded by LDA errors. Indeed, when the lattice constant of CuInS$_2$ is slightly reduced (say 4%), the calculated local moment is 4.0 $\mu_B$, and FM is also favored.

[24] P. Mahadevan and A. Zunger (unpublished).

[25] C. Kilic and A. Zunger, Appl. Phys. Lett. **83**, 2007 (2003).

[26] C. Kilic and A. Zunger, Phys. Rev. B **68**, 075201 (2003).

[27] N. Tsujii, H. Kitazawa, and G. Kido, Phys. Status Solidi A **189**, 951 (2002).

[28] P. Mahadevan and A. Zunger, Phys. Rev. B **68**, 075202 (2003).

[29] *LANDOLT-BÖRNSTEIN: Numerical Data and Functional Relationships in Science and Technology*, edited by K.-H. Hellwege (Springer, Berlin, 1980), Vol. III.